nELISA: A high-throughput, high-plex platform enables quantitative profiling of the secretome

Milad Dagher[1,3,4,*], Grant Ongo[1], Nathaniel Robichaud[1], Jinglin Kong[1,3,4], Woojong Rho[1,3,4], Ivan Teahulos[1,3,4], Arya Tavakoli[1], Samantha Bovaird[1], Shahem Merjaneh[1], Andrew Tan[1], Kiran Edwardson[1], Christelle Scheepers[1], Andy Ng[3], Andy Hajjar[1], Andy Lee[1], Philippe DeCorwin-Martin[1], Shafqat Rasool[1], JiaMin Huang[1], Yu Han[2], Srinivas Niranj Chandrasekaran[2], Lisa Miller[2], Maria Kost-Alimova[2], Adam Skepner[2], Shantanu Singh[2], Jeffrey Munzar[1], Anne E. Carpenter[2], David Juncker[3,4,*]

[1] Nomic Bio, Montreal, QC, Canada
[2] Broad Institute of MIT and Harvard, Cambridge, MA, USA.
[3] McGill University and Génome Québec Innovation Centre, Montreal, QC, Canada
[4] Biomedical Engineering Department, McGill University, Montreal, QC, Canada
* Correspondence: milad@nomic.bio; david.juncker@mcgill.ca

Abstract
We present the nELISA, a miniaturised, high-throughput, and high-fidelity protein profiling platform. DNA oligonucleotides are used to pre-colocalize antibody pairs on spectrally encoded microparticles and perform displacement-mediated detection while ensuring spatial separation between non-cognate antibody pairs. Read-out is performed cost-efficiently and at high-throughput using flow cytometry. We assembled an inflammatory panel of 191 targets that were multiplexed without cross-reactivity or impact to performance vs 1-plex signals, with sensitivities as low as 0.1pg/mL and measurements across the platform spanning 8 orders of magnitude. We then performed a large-scale PBMC secretome screen, with cytokines as both perturbagens and read-outs, measuring 7,392 samples and generating ~1.5M protein datapoints in under a week, a significant advance in throughput compared to other highly multiplexed immunoassays. We uncovered 447 significant cytokine responses, including multiple putatively novel cytokine responses, that were conserved across donors and stimulation conditions. We also validated its use in phenotypic screening, and proposed applications for the nELISA in drug discovery.

Introduction

Proteins are a fundamental part of biology, as the major effector class of molecules. It is thus crucial to quantify and analyse them to understand the state of a biological system and improve the detection and treatment of diseases[1]. While transcriptomics has been useful as a proxy for protein profiling, it has limitations due to post-transcriptional regulation, differential translation rates, protein degradation, and spatiotemporal regulation, among other phenomena [1]. Advancements in protein profiling methods could provide powerful new tools for biological research and drug discovery, if they can be scaled up and applied broadly from early discovery to the clinic.

Although various tools for protein analysis exist, it is complicated by issues such as large dynamic ranges, protein instability, and the lack of an amplification method. Significant efforts have been dedicated to developing scalable, high throughput, high sensitivity, and affordable proteomics, aiming at replicating the impact of next-generation sequencing in genomics [1]. However, lacking PCR and the ease of complementary probes of DNA makes such proteomic scaling more challenging.

Mass spectrometry-based proteomics can be useful for discovery in many contexts but have so far failed to overcome the severe trade-off between throughput and sensitivity, remain comparatively low in throughput, and are biassed towards high abundance proteins [1]. The sandwich immunoassay, commonly known as the ELISA (enzyme linked immunosorbent assay), remains a ubiquitous tool and approach for protein quantification from bench to clinic. However, multiplexing ELISA systems to capture significant portions of the proteome has been limited by reagent-driven cross-reactivity (rCR), which severely jeopardises assay fidelity, even at low- to mid-plex levels [2]. In fact, rCR is the major barrier to multiplexing immunoassays beyond ~25-plex. rCR is caused by the mixing of non-cognate antibodies, which are combined in solution and incubated together for target detection [2,5]. This mixing enables combinatorial interactions between all antibodies and proteins, and allows the formation of mismatched sandwich complexes, which can be formed as a result of a single non-specific binding event. These non-specific interactions increase exponentially as the number of antibody pairs in solution increases, and have so far limited the multiplexing of immunoassays to <50-plex, even with intensive selection of antibodies to minimise rCR [1,2,9].

Efforts to overcome or avoid these issues have been a focus for the last two decades, resulting in several developed, and developing, solutions. Commercially available platforms such as Olink's PEA technology [3] and Somalogic's SomaScan [4] allow more than 1,000 proteins to be measured in every assay. These platforms are increasingly used, despite comparatively high costs ($100s per sample), and throughput plateauing at <1000 samples per day. Furthermore, we previously reported methods to spatially array and separate miniature sandwich immunoassays so as to prevent antibodies from mixing and thus alleviating potential cross-reactivity. Our arrays required two spotting rounds, one to immobilise the capture antibody, and a second to co-localize the corresponding detection antibody following sample incubation and wash steps. These localised spots of cognate antibody pairs enabled detection of >100 proteins with high specificity [5,6]. This microarray approach was simplified by pre-spotting either capture or detection antibodies as microdroplets on separate chips that were mechanically aligned and pressed together, thereby fusing matched antibody pair droplets while avoiding non-cognate interactions. This chip-to-chip method enabled the detection of highly similar antigens, such as different isoforms of the same protein and post-translational modifications of proteins [7]. However, lengthy spotting protocols and technical challenges increased cost and limited the reproducibility and throughput, similarly to the limitations of PEA and SomaScan, which entail limited reproducibility and ability to scale in a cost-efficient manner. Thus, a platform that achieves specificity at scale without compromising other parameters such as throughput, cost-efficiency, and versatility has yet to be developed.

Here, we introduce the nELISA, a next-generation multiplexed bead-based assay platform that combines two technologies to achieve high-fidelity multiplexing at scale. The first technology is CLAMP (colocalized-by-linkage assays on microparticles), which we introduce here for the first time. CLAMP is a novel sandwich assay design that prevents cross-reactivity by pre-immobilizing antibody pairs on the surface of microparticles. We combine CLAMP with a large-scale encoding and decoding approach to bead-based flow cytometry assays that we previously described [8], creating the nELISA. As a first demonstration of the nELISA, we built a 191-plex secretome panel that targets low-abundance cytokines, chemokines, and growth factors. Here, we demonstrate its sensitivity, specificity and reproducibility, and illustrate the nELISA's potential for high-throughput screening (HTS) by profiling 191 proteins in 7,392 samples. This was achieved in less than 1 week, surpassing the throughput of other highly-multiplexed assays. We also illustrate the ease with which the nELISA can be integrated to existing HTS workflows by combining it with Cell Painting for phenotypic screening of a reference compound set. Finally, we demonstrate that the nELISA can not only recapitulate hundreds of expected immune phenotypes in a single experiment, but can also reveal unexpected insights with direct implications for drug discovery and development.

Results

CLAMP: a miniaturised sandwich assay on microparticles that inherently avoids reagent driven cross-reactivity in multiplexing.

To overcome the rCR and throughput limitations of multiplexed immunoassays, we developed the CLAMP, which miniaturises the ELISA assay at the surface of a bead. The bead-based nature of CLAMP achieves separation between non-cognate antibodies, each pair on their respective CLAMP, during the assay incubation step. It thus restricts sandwich binding of an antigen by cognate antibodies on the same bead, and precludes off-target interactions with non-cognate antibodies on other beads. Furthermore, unlike technologies based on aptamers, sequencing, microarrays, or droplets, this approach enables massive scaling due to the rapid and cost-efficient detection methods associated with bead-based technologies[10]: for example, fluorescently-labelled beads can be rapidly identified and quantified using commercially available flow cytometers such as the ZE5 (Bio-Rad), which enables processing of 384-well plates in 60 minutes at a cost of pennies per sample.

To achieve protein profiling at low cost and high-throughput without rCR, the CLAMP departs from the classical sandwich ELISA in three key ways: 1) pre-assembly of antibody pairs; 2) releasable detection antibodies; 3) conditional signal generation. First, antibodies are pre-assembled on their respective capture antibody-coated beads using flexible and releasable DNA oligo tethers (Fig. 1a). When samples are mixed with the beads, target proteins can be recognized simultaneously by the antibodies, forming a tertiary sandwich structure (Fig. 1b). Second, the releasable tethering of the detection antibodies allows for their displacement by complementary DNA oligonucleotides with longer sequences than the tethering sequence. Thus, CLAMP uses a novel signal transduction mechanism with

a detection-by-displacement protocol based on toe-hold mediated strand displacement (Fig. 1c). Third, fluorescently labelling the displacement oligo results in conditional signal generation. Indeed, only target-bound tertiary sandwich complexes are both labelled by the fluorophore and remain bound at the surface of the bead. In contrast, non-displacement isn't associated with a fluorescent signal, whereas target absence, or non-specific interactions, result in washing away of the fluorescent signal, thus ensuring low background signal.

Of note, during the displacement step, antibodies released from the bead and present in solution are found at concentrations 1000x lower than that required to form off-target complexes. Indeed, while the local-concentrations at bead surfaces can be in the micromolar range, the use of a low number of target-specific microparticles, and the limited number of antibodies present at the surface of each bead, result in a bulk concentration of detection antibody in solution too low (<pM) to yield any off-target binding. Thus, as a result of its unique structure and detection method, CLAMP inherently avoids reagent driven cross-reactivity in multiplexing. In addition, the CLAMP format dramatically reduces the amount of detection antibodies consumed, relative to other multiplexing formats; considering that reagent costs are the main driver of the high cost associated with protein profiling tools, the low reagent costs of CLAMP result in significant advantages in cost-efficiency.

The nELISA combines CLAMP with emFRET to achieve high levels of multiplexing and throughput

To fully leverage the multiplexing capacity unleashed by the rCR-free nature of the CLAMP, we combined it with our previously-developed fluorescent barcoding technique [8], which achieves large-scale encoding and precise multi-colour labelling of beads. The technique leverages an ensemble multicolour FRET (emFRET) model to achieve facile encoding and decoding despite stochastic multicolour energy transfer. The use of four fluorescent dyes with partially overlapping spectra at various concentrations enables distinction of ~2,300 barcodes, and can be further expanded via optimization or inclusion of additional dyes. As a result, the nELISA has the potential to profile thousands of proteins in each sample. Furthermore, the fluorescence-based readout enables the use of high-throughput flow cytometry, and the use of 384-well plates to achieve high-throughput protein profiling. We developed two workflows enabling 1,536 wells to be analysed either in a single day, or over 2 days with normal working hours, which is, to the best of our knowledge, the highest throughput of any highly-multiplexed immunoassay.

Fidelity of assay performance is maintained at high-plex

To demonstrate high-fidelity multiplexing, we assembled a comprehensive secretome panel selecting 191 targets including cytokines, chemokines, and growth factors (Suppl. Table 1). Secreted proteins were chosen as the first set of proteins because they are simultaneously important to study, difficult to measure, and can have complex interactions and context-dependent effects that require broad profiling to fully understand. To determine whether multiplexing had any negative effect on protein quantification, we ran a head-to-head measurement comparing signals generated in single-plex vs 191-plex. For individual proteins, calibration curves were indistinguishable; across the 191-plex panel, measurements correlated with an R^2 of 0.988 (Fig. 2b). Thus, nELISA measurements are insensitive to multiplexing.

We then screened for rCR by running 'spike-one-in' testing, where each recombinant antigen was separately spiked to detect any cross-reactive detection by non-cognate CLAMPs (Fig. 2c). We also ran 'leave-some-out' testing, in which antigen pools lacking a subset of nELISA targets were profiled to ensure rCR remained low in the presence of complex protein solutions (Fig. 2d). Of the 36,000+ possible cross-reactivities (where protein x is detected when protein y is spiked), we only detected 5; of these 3 were explained by shared epitopes. For example, it was expected that an IL-12 p40-specific CLAMP would detect IL-12 p70 and IL-23, as these heterodimers both contain the IL-12 p40 subunit. It was also expected that CXCL12 alpha and CXCL12 beta CLAMPs would detect both CXCL12 isoforms, as they differ by only 4 residues. Unexpectedly, the CCL13 CLAMP detected CCL17, and the CCL3 CLAMP detected PCSK9. These cross-reactivities are presumed to be due to poor antibody specificity, whereby both antibodies detect the same off-target and would yield cross-reactive results even in a standard ELISA, and can be addressed by selecting alternative antibody pairs. These results indicate virtually complete specificity and accurate quantification of our 191-plex secretome panel, demonstrating that the nELISA fidelity is unaffected by multiplexing well beyond the traditional limit imposed by rCR.

Characterization of dynamic range, sensitivity, and precision

To further characterise the performance of the nELISA in 191-plex, we analysed standard curves generated for each nELISA target. nELISA thermodynamics and kinetics are such that the dose-response curve is sigmoidal and is robust against the Hook effect (Fig 2e). Thus, quantifications near the upper limits of detection are robust. These characteristics enabled us to extend the dynamic range (xDR) of the assay by merging concentrations obtained from profiling proteins at multiple dilutions (see Methods), without impacting the assay throughput (Fig. 2e-f). Thus, high abundance proteins with concentrations up to 10ug/mL could be quantified accurately. At the lower end of the detection spectrum, we analysed the sensitivity of the nELISA, and found limits of detection ranging from low pg/mL to ng/mL (Fig. 2g). These were driven primarily by antibody affinities, with their affinities in the CLAMP format in line with their reported affinities in single-plex ELISA format. The most sensitive CLAMPs could detect low abundance proteins with concentrations as low as ~0.1pg/mL. Combined with our xDR method, the nELISA thus yielded a total protein quantification range of 8 orders of magnitude, with each CLAMP possessing a dynamic range of 3-6 orders of magnitude. Importantly, nELISA performance was highly reproducible. By measuring the same sample across wells, plates and profiling days, we calculated that the coefficient of variation (CV) of each CLAMP was ~3% well-to-well, and 5% plate-to-plate and day-to-day (Fig. 2h).

Benchmarking and validation against Luminex

To validate the nELISA ability to quantify proteins from biological samples, we collected cell culture supernatants from stimulated peripheral blood mononuclear cells (PBMCs), which we profiled with the nELISA, and with a 48-plex panel based on the more traditional multiplexed immunoassay platform, xMAP. Of the 36 targets shared by both platforms, 24 were detected in our samples by both platforms. Quantification of these targets revealed that xMAP and nELISA results correlated quite well, with a median Spearman correlation of 0.92 (Fig 2i, Suppl. Fig. 1). Leave-some-out testing revealed that targets correlating poorly between nELISA and xMAP were due to rCR in the xMAP platform (Fig 2j). These results demonstrate that the nELISA is unique in its ability to achieve bona fide multiplexed quantification, where concentrations measured are not impacted by the level of multiplexing.

A PBMC secretome screen to characterise cytokine responses

A comprehensive cytokine panel that can efficiently be used in high-throughput has numerous applications in drug discovery, medicine and diagnostics. A common challenge to all these applications is that intercellular signalling via cytokines is complex due to (a) pleiotropy and redundancy of signalling pathways, (b) technical difficulty to measure at scale and systematically due to low throughput and high cost of existing techniques, and (c) extensive post-transcriptional and post-translational regulation of cytokines limiting the correlations between mRNA and protein levels.

To demonstrate how the multiplexing, throughput and cost-efficiency of the nELISA can be used to more broadly characterise cytokine activity, we studied a variety of secretory responses from human PBMCs. We selected 6 different PBMC donors to capture biological variability, which we treated with 4 different inflammatory stimuli at multiple doses. In addition, we used a small library of 80 recombinant human proteins with known immunomodulatory properties as “perturbagens” to further characterise immune responses (Fig 3a), generating 7,392 profiles of human cytokines, chemokines, and growth factors. Using UMAP as an overview of the entire nELISA dataset, distinct phenotypes clustered by stimulation condition, by PBMC donors, as well as by the concentration of stimulus used (Fig 3b). In addition, individual cytokine perturbagens with particularly strong effects created their own phenotypic clusters, including IL-4, IL-10, IL-1 RA/RN, IFNa2 and IFNb (Fig 3b), demonstrating the power of the nELISA for phenotypic screening.

nELISA recapitulates classical immune responses

Using different stimulatory agents enables preferential stimulation of different subsets of cells (T cells vs myeloid cells) within PBMCs. These generally well understood inflammatory responses were clear in the dataset. Thus, primarily myeloid cell-derived proteins such as IL-1 alpha and IL-1 beta increased in response to myeloid stimuli (Fig. 3c), whereas primarily T-cell derived proteins like IL-17A and IL-2 increased in response to T cell stimuli (Fig. 3d);

proteins expressed by multiple cell types such as TNFa and IFNg increased in response to all stimuli (Fig 3c-d). Next, we analysed cytokine interactions, defined as changes in expression of a given PBMC-derived cytokine in response to a given recombinant cytokine perturbagen, in any or all of the stimulation conditions, across multiple donors (see Methods). Classical pro-inflammatory cytokines such as IFNg and IL-1b were regulated by a variety of perturbagens, in a manner consistent with the expected role of each perturbagen (Fig 3e-f). For example, IFNg increased in response to IFNa2/b, IL2, IL-18, Il-15, and IL-7, all powerful inducers of IFNg [11–14], but was suppressed by IL-4, IL-10 [15,16].

To further establish that the nELISA can recapitulate expected biology, we compared the cytokine interaction responses found with the nELISA against CytoSig, a database of consensus, data-driven, cytokine-activity transcriptomic signatures [17]. Differences between mRNA and protein measurements notwithstanding, well-established immune responses were expected to be represented in both datasets and provide cross-validation. We found a total of 449 cytokine interactions using the nELISA in our own PBMC screen, and 137 cytokine interactions in PBMC data from CytoSig, of which 45 were detected by both platforms. Of these, 87% were in agreement with respect to directionality: 29 interactions resulted in increased cytokine production, and 10 resulted in repressed responses, in both nELISA and CytoSig (Fig 3g). These included well known responses such as the induction by IFNg of the IFNg-inducible chemokines CXCL9 and CXCL10, and the potent immuno-stimulatory effects of IL-15, which induced both adaptive and innate immune mediators such as IFNg, TNFa, CXCL9, CXCL10, CCL5, IL-17F, IL-22, and IL-1b, among others (Fig 3g).

nELISA reveals cytokine interaction insights beyond transcriptomics

Interestingly, CytoSig data lacked many hallmark effects of Th1 and Th2 modulators. For example, the potent inhibitory effect of the Th2 cytokine IL-4 on IFNg, TNFa and IL-1b was missing, as was its ability to induce CCL22 and CCL24 [15,18–20] (Fig 3e). In fact, nELISA detected many more interactions in PBMCs than CytoSig (449 vs 137). Much of the difference stems from the inclusion of inflammatory stimuli in the nELISA dataset, enabling the detection of suppressive effects on cytokines with low baseline expression. As a result, CytoSig interactions are primarily increased expression (81%), whereas nELISA data is more balanced. This may explain why CytoSig fails to detect much of the potent anti-inflammatory effects of IL-10 on IFNg, TNFa, IL-1b, IL-12 p40, CCL1, CCL3, CCL4, CCL5, CCL19, CXCL5, G-CSF, MMP-1, etc. [21] (Fig 3g).

Furthermore, CCL5, a particularly IFNg-sensitive protein, was induced in the nELISA dataset by recombinant IFNg and several conditions leading to increased IFNg. However, its induction by IL-2, IL-7, IL-18, and IFNa2/b was not detected by CytoSig (Fig 3g). This may be due to post-transcriptional induction of CCL5 by IFNg[22,23], or may reflect differences in experimental setup, such as temporal differences that would preclude detection of secondary effects by CytoSig. Similarly, post-transcriptional regulation likely explains differences in IL-1b regulation seen in nELISA vs CytoSig. Indeed, IL-1b is primarily regulated by cleavage and release of a pre-synthesized precursor, rather than de novo transcription [24], rendering protein-based detection methods critical. In line with this, IL-1b was the most responsive protein in the nELISA PBMC screen, responding to 35 distinct cytokine perturbagens, but only responding to IL-15 and IFNb in the CytoSig database (Fig 3g). This type of cytokine post-transcriptional regulation is likely the source of the few disagreements between nELISA and CytoSig data. As seen in Fig 3g, there are 6 examples of a cytokine interaction resulting in a decrease in nELISA protein data, but an increase in CytoSig mRNA data. These interactions involve the expression levels of TNFa, IL-1a, CCL2, and CXCL1, all of which are well-studied examples of cytokines regulated at the level of translation into proteins, as well as mRNA stability [25–28]. Thus, the nELISA recapitulates well established biology captured by gene expression databases such as CytoSig, in addition to providing protein-level information that is overall a more accurate representation of cell states at the population level.

nELISA is compatible with - and complementary to - high-content phenotypic screening

Profiling the secretome using nELISA is in theory compatible with a wide variety of cell-based assays, by first removing the cell supernatant for nELISA and using remaining cells for any cell-based assay of interest, including other multiplex profiling assays probing mRNA, chromatin, or morphology. This could increase information content from a single sample. We tested Cell Painting, an image-based assay where microscopy captures images of cells stained with six dyes that label eight cellular components

(https://www.biorxiv.org/content/10.1101/2022.07.13.499171). Thousands of image-based features are then extracted to form an image-based profile of the sample.

Using samples of A549 cells (human lung adenocarcinoma) being prepared by the JUMP-Cell Painting Consortium (https://www.biorxiv.org/content/10.1101/2023.03.23.534023), we confirmed compatibility of nELISA with Cell Painting by measuring secretome profiles from the exact same samples that were then Cell Painted. These cells were treated with a library of 306 well characterised compounds from the Broad Institute's drug repurposing library [20]. We tested the ability of each assay to identify compounds with shared mechanisms of action (MOA) and gene targets.

We first determined the "self-retrieval" of each compound on both platforms, representing the ability of replicate wells of a compound treatment to differentiate each other's phenotypes from that of control wells. Said differently, compounds with high self-retrieval yield a strong and distinct enough impact on the measured phenotype as compared to control well. Among compounds resulting in significant self-retrieval, nELISA and Cell Painting were able to retrieve MOA and gene target information based on shared phenotypes, with MOA-retrieval rates of 21-27% and gene target retrieval rates of 15-16%, respectively, though more total compounds were self-retrieved by Cell Painting (Suppl. Fig. 2). Interestingly, the two platforms yielded complimentary results, with each providing better predictions for distinct sets of compounds, in addition to a shared subset of compounds with MOA/gene targets retrieved by both platforms. For example, inhibitors of protein synthesis and microtubule targeting compounds were also well predicted by both platforms. Thus, we validated our ability to run two richly informative profiling assays on the same physical samples, and to cluster individual chemical perturbagens according to their mechanism of action or gene target.

nELISA profiles reveal compounds and cytokines with shared response profiles

In the nELISA dataset, analysing the similarity of A549 response profiles (see Methods) to inhibitors of protein synthesis revealed that these compounds formed a distinct cluster characterised by a general decrease in secreted proteins, including IL-11, CXCL16, and VEGF-A (Suppl. Fig. 3). These compounds can induce ER stress due to accumulating misfolded proteins, which can result in an inflammatory response [37]. They also led to a paradoxical induction of MIF. Of note, MIF, unlike most cytokines, is produced constitutively and is released from pre-formed cytoplasmic stores, and can thus be secreted despite inhibition of protein synthesis [30]. As MIF has been reported to play a role in the response to ER stress by acting as a chaperone for SOD1, our nELISA results may provide mechanistic insight into the response of A549 cells to these drugs [38]. Another example of mechanistic insight provided by nELISA phenotypes came from inhibitors of extracellular proteases, such as the matrix metalloprotease inhibitor batimastat. These compounds were well predicted by nELISA and resulted in reduced detection of the soluble forms of typically membrane-bound proteins, such as CXCL16, TNF RI and amphiregulin, likely due to inhibition of the proteases leading to their cleavage and shedding from the cell surface in control samples (Suppl. Fig. 3).

We also applied our response profile similarity analysis pipeline to our PBMC screen to identify phenotypes specific to the perturbagens, rather than to the donors and stimulus conditions. We therefore calculated the fold change in expression of each protein in our 191-plex panel, in response to each of the cytokine perturbagens, across all donors within a stimulus condition (Suppl. Fig. 4). We also compiled effects across all stimulation conditions to capture the most reproducible perturbagen effects. UMAP clustering highlighted the most similar perturbagens (Fig 4a), with the protein expression patterns underlying these clusters shown in Fig 4b. It should be noted that some of our observations may derive from the purity of the recombinant proteins used, and the potential presence of bacterial contaminants; however, this effect is likely minor, as most cytokines cluster in predictable ways.

Thus, classical Th1/Th2 immune responses clustered around the prototypical cytokines IFNg and IL-4, and their induction of IFNg/CXCL10/CCL5, or CCL17/CCL22/CCL24, respectively (Fig 4a). The proximity of these clusters is explained by the shared inhibition of innate immune responses (ex: IL-1b, TNFa, G-CSF) as seen in Fig 4b. An additional cluster that shared the suppression of IL-1b/TNFa, but had little to no effect on the expression of other cytokines, was formed by recombinant C5/C5a, EMMPRIN, GDNF, MMP-3, MMP-7, uPA, PTX3, and the soluble form of FAS-L. A distinct cluster was formed of cytokines whose main effect was to induce IFNg expression; this included the interleukins IL-2, 7, 15, 18, 23, 27 as well as CXCL12beta. Interestingly, CXCL12alpha clustered with another group of proteins whose main effect was to induce the secretion of IL-1b (Fig 4-b). This is the largest group and

included IL-1a, LIF, IL-33, PDGF-BB, sCD40L, CCL21, TRAIL and IL-17C/D/F. The remaining clusters were formed by perturbagens either inducing TNFa, IL-10 and IL-1a/b, or blocking TNFa and/or CCL24.

Interestingly, our analysis pipeline enabled us to highlight lesser known cytokine biology, such as chemotaxis-independent effects of chemokines [39]. Thus, CX3CL1, CCL1, CCL5, CCL11, CCL26, CXCL10, CCL24, CXCL12alpha/beta and C5a all modulated the expression of cytokines such as IFNg, TNFa, IL-1b, GM-CSF and IL-10, in the absence of a chemotactic gradient (Fig 4b). These observations support a growing body of evidence for activities of chemokines beyond migration [40]. More specifically, the nELISA captured subtle functional differences between related chemokines, as we identified differences between the response to CXCL12alpha and CXCL12beta, despite these proteins differing by only 4 residues [41,42]. Thus, CXCL12alpha primarily induced IL-1b, whereas CXCL12beta primarily induced IFNg. CXCL12beta also blocked CCL24 expression, which was not seen with CXCL12alpha. The two isoforms also displayed distinct, stimulus-specific effects (Suppl. Fig. 4). Our results are consistent with other functional assays showing differences in the activity of CXCL12alpha and beta [41–43]. This may indicate that the alpha and beta isoforms preferentially signal via different G-protein signals. In fact, the CXCL12 receptor, CXCR4, can signal through a variety of G-proteins, in addition to beta-arrestin and JAK/STAT [44]. For example, CXCL12alpha has been described as a co-stimulatory signal for T cells functioning through distinct G-protein signals (G_q and G_{11}) than those classically associated with chemotaxis (G_i) [45].

Of note, nELISA clustering enabled identifying similarities between therapeutic cytokines, suggesting possible drug repurposing approaches. IL-1 Receptor antagonist (IL-1 RARN) and IFNb clustered similarly based on their inhibition of innate immune responses, yet IL-1 RARN induced none of the pro-inflammatory cytokines induced by IFNb, such as IFNg and CXCL10 (Fig 4a-c). This may have implications in the treatment of multiple sclerosis (MS): indeed, IFNb is a common treatment for MS that appears to function at least in part through increasing IL-1 RARN expression, but has flu-like side effects [31–33]. In contrast, recombinant IL-1 RARN (anakinra) is very well tolerated and is currently being evaluated for MS in a phase 1 clinical trial [34,35]. In our data, IL-1 RARN was induced by IFNb, but itself displayed only anti-inflammatory effects. In fact, correlating the effect of adding IFNb or IL-1 RARN to PBMCs demonstrates that IL-1 RARN can inhibit all of the same cytokines/chemokines as IFNb, with the exception of CCL22 and CCL24, while additionally inhibiting the expression of cytokines induced by IFNb but thought to be detrimental to MS, such as IFNg and CCL7 (Fig 4c). Thus, our screen provides support for using anakinra in MS, and highlights the power of nELISA protein profiling for drug discovery.

Discussion

Here, we have shown that the nELISA overcomes the rCR limitations seen with other multiplex immunoassay systems, enabling scaling of content to 191-plex and beyond. The nELISA also miniaturised the sandwich immunoassay, enabling scaling of throughput to ~10,000 samples per week. All while maintaining or improving on the sensitivity, specificity, and dynamic range of the gold-standard ELISA assay. We applied the nELISA to HTS, where we demonstrate that the platform can report on the activity of small molecules and recombinant proteins. In fact, the nELISA is compatible with all kinds of perturbagens, including CRISPR gene modulation, therapeutic antibodies, and a wide variety of engineered proteins such bi-specific engagers and CAR T constructs. We have shown that the nELISA captures expected cellular phenotypes and biological interactions that provide critical insights for drug discovery. For example, in our PBMC assay, the clear separation of responses by donor suggests powerful uses for the nELISA in functional genomics if scaled to larger cohorts, as done in the Human Functional Genomics Project [36].

The throughput and cost-efficiency achieved with the nELISA is a major advancement for secretome analysis. Other highly multiplexed assays such as PEA (Olink) and SomaScan (SomaLogic) lack the throughput and cost-efficiency to profile cell culture supernatants at the scales reported here. Even methods such as transcriptomics are limited by the amount of cellular material, the cost, and the time required to extract and purify mRNA. In contrast, nELISA yields results from 1536 samples in 1-2 days from sample collection, greatly increasing the wealth of data from secreted proteins available in HTS. We highlight additional advantages of proteomics over transcriptomics. For example, the key inflammatory mediator IL-1b was the most regulated protein in our screen; because it is post-translationally regulated, none of these responses would have been detected by transcriptomic assays. Secondary effects are also more difficult to discriminate in transcriptomic datasets. Indeed, secretome profiling is compatible with repeat sampling from the same well, enabling the tracking of cellular phenotypes over time and the deconvolution of primary

effects from those further downstream. Such an experiment would enable unambiguous determination of whether CCL5 is induced downstream of IFNg, an option that would require an unwieldy multiplication of samples for methods requiring cell lysis or fixation, such as transcriptomics.

However, nELISA analysis doesn't preclude transcriptomics analysis from the same samples; in fact, the 191-plex secretome panel has the advantage of being easily amenable to combining to other cell-based assays, such as transcriptomics or Cell Painting. Our results demonstrate that such tools can be combined to provide additional biological insights. Thus, nELISA and Cell Painting provided complimentary phenotypic insights, with the nELISA also providing mechanistic insight, as seen for inhibitors of protein synthesis or inhibitors of proteases. This highlights the potential for combining nELISA with a wide range of cell-based assays to provide additional insights. In addition to transcriptomic or morphological assays, nELISA can be combined with functional assays such as cell killing assays common in immuno-oncology settings, or cell surface staining experiments prevalent in immunology.

Finally, the nELISA's ability to distinguish between related chemokines would have particularly useful applications in the development of therapeutic chemokines: indeed, screening with a chemotaxis assay is significantly more challenging, with lower throughput and signal-to-noise, than screening on the basis of changes in protein expression [46,47]. In the case of CXCL12 isoforms, identifying secreted biomarkers of alternatively activated receptors could thus provide greater power to identify and optimise drug candidates. More generally, the ability of the nELISA to capture distinct effects of perturbagens with minimal sequence/structure differences highlights its potential utility to screen structure-activity relationships. Thus, the nELISA is a uniquely valuable tool for drug discovery that yields high quality protein data, at scale, and in a format amenable to combining with other screening assays.

Conflict of Interest Statement

The Authors declare the following competing interests: N.R., G.O., W.R., I.T., A.T., J.K., J.M. and M.D. are employees and have ownership interest in Nomic Bio, which markets the nELISA platform, D.J. has ownership interest in Nomic Bio. S.S. and A.E.C. serve as scientific advisors for companies that use image-based profiling and Cell Painting (A.E.C: Recursion, S.S.:Waypoint Bio, Dewpoint Therapeutics) and receive honoraria for occasional talks at pharmaceutical and biotechnology companies. All other authors declare no competing interests.

Acknowledgements

We thank Daniel Graham and Sarah Headland for their invaluable insights into the biology captured by nELISA profiling of PBMCs. We also thank the High-Throughput Screening Core Facility of the Institute for Research in Immunology and Cancer of the Université de Montréal for culturing and high-throughput screening of PBMCs.

Funding

Funding for this study was provided by Nomic bio. Additional funding was provided by the Natural Sciences and Engineering Research Council of Canada (NSERC) Discovery and I2I grants, as well as from the Consortium Québécois sur la Découverte du Médicament (CQDM), Healthy Brains Healthy Lives (HBHL) and GSK. The authors also acknowledge funding from the Massachusetts Life Sciences Center Bits to Bytes Capital Call program (to AEC) and the National Institutes of Health (R35 GM122547 to AEC). The authors also gratefully acknowledge the use of the PerkinElmer Opera Phenix® High-Content/High-Throughput imaging system at the Broad Institute, funded by S10 Grant NIH OD-026839.

Methods

Recombinant sample generation

Recombinant protein stocks and protein pools (Nomic Bio) were prepared in Sample Buffer, consisting of RPMI + 10% FBS, containing 1-191 proteins at 100ng/mL per protein. For standard curves in singleplex and in multiplex, individual protein stocks and protein pools were serially diluted in Sample Buffer from 100ng/mL to 0.1pg/mL per protein. For "Spike-1-in" assays, individual protein solutions were prepared at 10 ng/mL. For "Leave-some-out" assays, protein pools containing 130-191 proteins at 100 pg/mL per protein were prepared in Sample Buffer. Each pool contained either all the targets in the 191-plex panel, or lacked a subset of targets in the 191-plex panel. For cross-reactivity comparisons with xMAP, protein pool A4 was serially diluted from 200ng/mL to 0.1pg/mL (per protein), and aliquots were stored at -80oC for profiling by nELISA and xMAP platforms. For reproducibility testing, a reference cell culture supernatant sample was distributed across the wells of four 384-well plates; for each plate,

nELISA profiling was performed on a different day, and variation was calculated across wells on the same day, and across plates on different days.

Dynamic Range extension (xDR)
To extend nELISA dynamic ranges, samples were profiled at 2 dilutions, 2X and 50X, and merged together before read-out by cytometry. Standard curves were extended by stitching the linear ranges of a real standard curve and a virtual, 25x diluted, standard curve. The sum of interpolated protein concentrations from the 2X and 50X dilutions was used to derive a single protein concentration for each sample.

Cell culture
Frozen PBMCs from healthy donors (StemCell) were thawed in 37oC water bath and transferred to 50mL Falcon tube with 40mL pre-warmed medium (RPMI + 10%FBS), centrifuged 10min@200g, then resuspended in 10mL pre-warmed medium. Viability was assessed by trypan blue exclusion (>95% viability for all donors) and 50,000 viable cells (25uL at 2M cells/mL) were transferred to each well of a 384 well plate, containing 50uL per well of pre-warmed media +/- stimulus +/- perturbagens, and incubated for 24h at 37oC. Perturbagens (Nomic Bio) were present at 50ng/mL. For stimulation conditions, LPS (InvivoGen) was present at 5ng/mL, 100ng/mL or 2000ng/mL; PolyIC (InvivoGen) was present at 400ng/mL, 2,000ng/mL, or 10,000ng/mL; ConA (InvivoGen) was present at 5ng/mL, 2,500ng/mL or 12,500ng/mL; for PMA/i (InvivoGen), PMA was present at 100ng/mL or 500ng/ml, while ionomycin was present at 1ng/mL or 5ng/mL.

Preparation, incubation and collection of cell supernatants from PBMCs was performed at the High-Throughput Screening Core Facility of the Institute for Research in Immunology and Cancer of the Université de Montréal. After 24h, supernatants were collected, aliquots were frozen and shipped on dry ice for nELISA profiling at Nomic's facilities or xMAP profiling at EVE Technologies facilities.

A549 cell culture was performed at the Broad Institute's Center for the Discovery of Therapeutics (CDoT). Cells were seeded in 4 replicate 384 well plates and cultured for 24h in DMEM + 10% FBS in the presence or absence of reference compound library. Compounds were present at a single dose (5uM). Supernatants were collected, frozen, and shipped on dry ice to Nomic's facilities for nELISA profiling. Cells were fixed and stained for Cell Painting as previously described [48].

Protein profiling
Samples of recombinant proteins or cell culture supernatants profiled using the nELISA were frozen and shipped on dry ice to Nomic's Montreal facilities and analysed using the Maxplex (191 targets) and standard protocols. Briefly, samples were thawed on ice and diluted as required with cell culture media, then mixed 1:1 with resuspended nELISA beads and incubated 3 hours at room temperature. Target-bound beads were washed with Wash Buffer, then resuspended in Assay Buffer. Displacement Oligo was added to beads and incubated 30 minutes at room temperature, followed by an additional wash and resuspension in Assay Buffer for readout by high-throughput cytometry (Bio-Rad ZE5 cell analyzer). Results were decoded using Nomic software. Samples profiled using the xMAP platform were shipped frozen to EVE technologies and analysed using the Human Multiplex Cytokine Array / Chemokine Array 48-Plex (HD48) and standard protocols. Standard curves for all targets were generated to derive pg/mL values from cytometry fluorescence units.

Data analysis pipeline - Fold change analysis
To identify compounds with significant effects on A549 cells, we calculated the fold change in expression of each protein in the 191-plex over the levels in control wells. Proteins with a fold change > 1.5 and $p < 0.05$ by Student T-test in any sample were considered significant; considering the exploratory nature of the experiment, no statistical correction was performed for multiple testing. Using the median value of the significant responses, clustergrams with hierarchical clustering were generated using cosine similarity ((python package: seaborn). UMAPs of the median fold change values were generated using cosine similarity dimensions=2, spread=1.3, minimum distance=0.2, nearest neighbours=4,python package: scanpy).

To identify cytokine interactions in our PBMC assay, we accounted for stimulus- and donor-specific effects as follows. For each perturbagen in each stimulus/stimulus concentration condition, the median concentration of each secreted

protein across donors was divided by the median concentration of donors in the same stimulus/stimulus concentration condition, but the absence of perturbagen, to obtain the fold change of all targets in response to all perturbagens in each condition. Significant cytokine interactions were defined by a fold change > 1.5 and $p < 0.05$ by Student T-test; considering the exploratory nature of the experiment, no statistical correction was performed for multiple testing. In addition, for all significant cytokine interactions, the median fold change across all stimulation conditions was calculated to identify cytokine interactions common across stimulus conditions. Clustergrams with hierarchical clustering were generated using cosine similarity and the default parameters included in the Seaborn python package. UMAPs were generated using cosine similarity with dimensions=2, spread=0.9, minimum distance=0.8, nearest neighbours=4 and the scanpy python package.

To correlate significant cytokine interactions with the CytoSig database, we identified recombinant perturbagens and responding genes/proteins that were shared in both datasets to limit comparisons to shared experimental conditions. We also limited comparisons to experiments compiled in CytoSig that were generated using PBMCs to avoid cell-type specific distinctions. Furthermore, only “high confidence” datasets were included in our analysis. For each cytokine interaction, consisting of a recombinant perturbagen and a resulting significant Fold Change in the expression of a PBMC-derived cytokine, nELISA and CytoSig results were correlated.

Evaluating retrieval performance of NELISA and Cell Painting

We use average precision (AP) to report the ability of nELISA and Cell Painting to predict chemical mechanisms of action. Average precision is an information retrieval metric that evaluates the effectiveness of a ranking system by calculating how accurately the system ranks items based on their relevance to a query.

We use average precision for two different tasks 1) the ability of each perturbagen to retrieve its own replicates from among negative control profiles (“self-retrieval”), and 2) the ability of each perturbagen to retrieve its sister compounds (i.e., compounds that share at least one common MOA or gene target) (“MOA retrieval” and “gene target retrieval”). We note that many compounds have multiple MOA and gene annotations rather than just one of each; in addition to the fact that annotations can be incorrect and incomplete, this makes the retrieval problem challenging. Formally, AP is the weighted mean of precision values across all ks, where k is the number of neighbours for a given class. The definition of class varies – each *perturbation* is the class while computing AP for task 1, and each *MOA* or *gene targeted by the compound* is the class for computing AP for task 2.

We measure similarity between perturbations using cosine similarity. Finally, we average AP per class, termed *mean Average Precision (mAP)* (for that class). For task 2, we first filter out those perturbations that cannot be retrieved relative to negative controls in task 1 and remove classes with only a single member. To set the threshold, we first calculate the p-values of each mAP in task 1 using a permutation test; compounds with a significance level of less than 0.05 are discarded. We summarise the success rate of a task by calculating the fraction of classes that have a p-value > 0.05

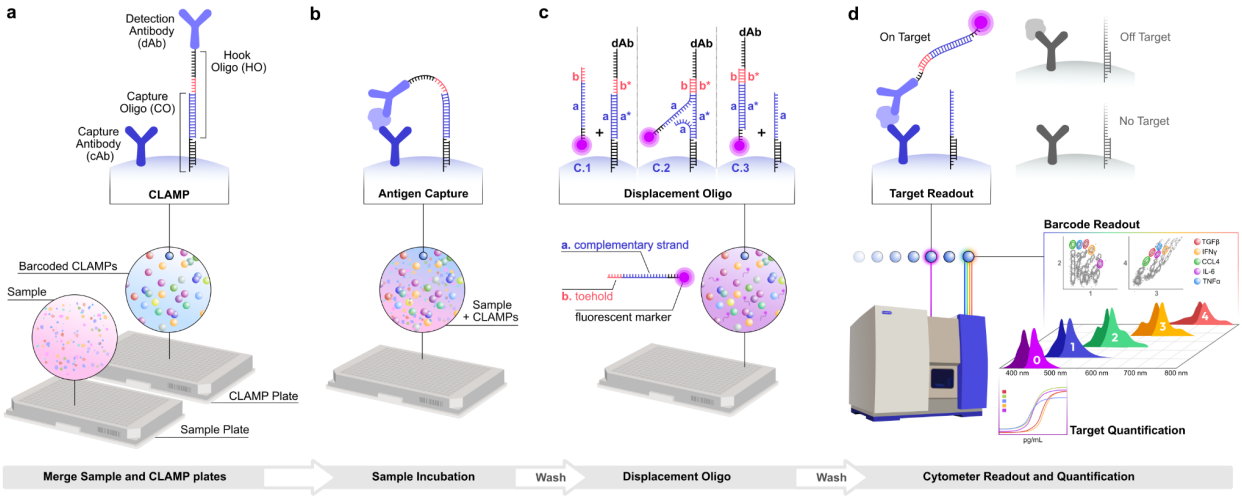

Figure 1. nELISA architecture and workflow. (a) A multiplexed nELISA is set up by pooling barcoded CLAMPs against different targets together. On each barcoded CLAMP, the detection antibody (dAb) is bound to a hook oligo (HO) that is tethered to the surface via partial hybridization with a capture oligo (CO) strand. (b) The assay is carried out by incubating the biological sample with barcoded CLAMPs generating sandwich binding in the presence of the target analyte only. (c) After washing, a fluorescently-labelled displacement oligo (DO) is added to displace HOs from their pre-hybridized COs via toe-hold mediated displacement, leading to (d) labelling of the sandwich complexes that remain on the surface. (bottom) Plate-based experimental workflow (from left to right): samples and nELISA beads in 384-well plates are combined, antigens are bound by cognate CLAMPs, displacement and labelling occurs on all beads in each well, beads are decoded and targets quantified by high-throughput flow cytometry. Fluorescence spectra of detection dye (0) and barcoding dyes (1-4) are shown.

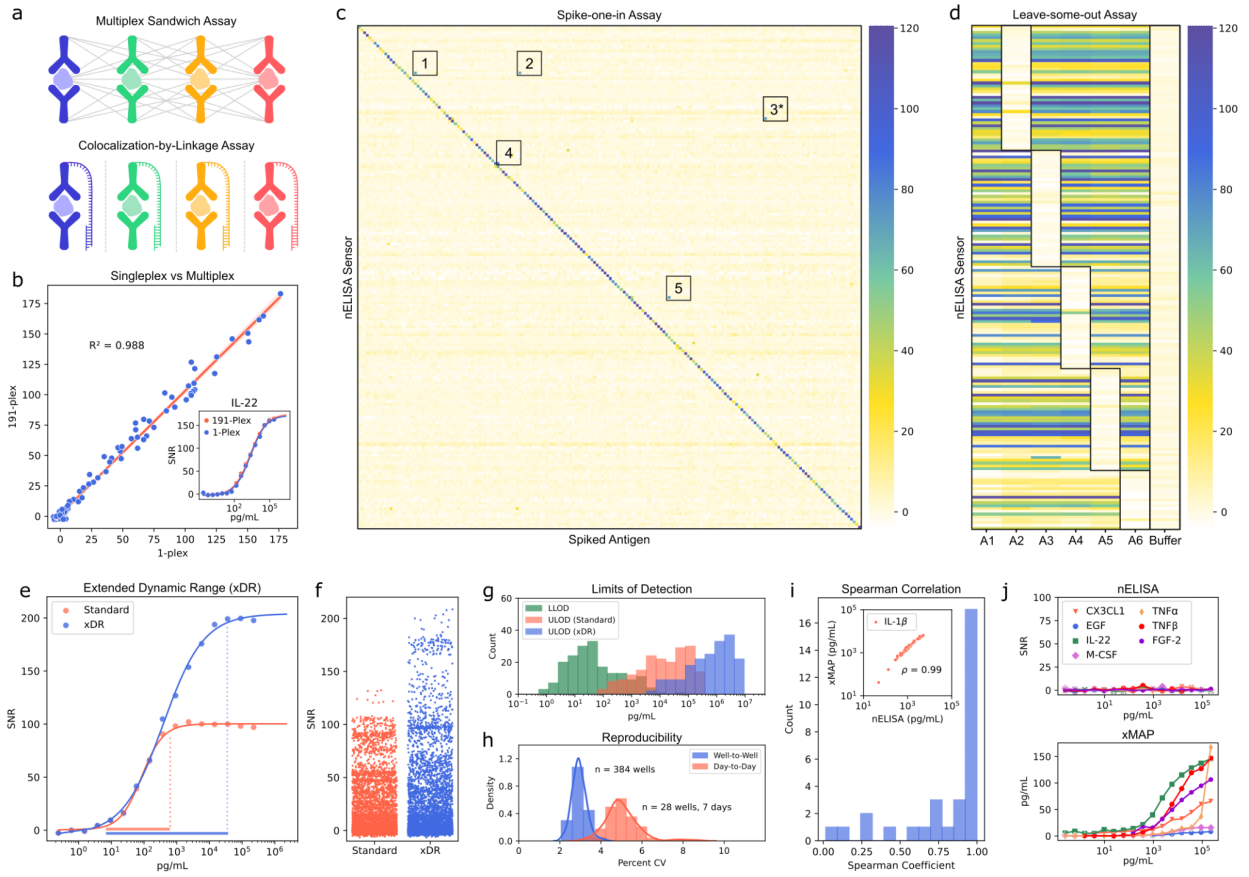

Figure 2: Characterization of the nELISA specificity, sensitivity, and reproducibility. (a) Schematic representation of cross-reactivity arising between reagents in traditional multiplexed ELISA formats, and its abrogation in the Colocalization-by-linkage format. (b) Correlation of SNR values for nELISA sensors used in isolation as a 1-plex (Singleplex), or in parallel with all the other sensors in the 191-plex nELISA panel (Multiplex); also shown is an example standard curve for IL-22 in 1-plex and 191-plex format (inset). (c) Spike-one-in assay, heatmap displays SNR values for each nELISA sensor in the 191-plex (y-axis) for each individually spiked antigen (x-axis); diagonal displays specific signals, cross-reactive events are numbered: 1) CCL13 sensor detects CXCL16; 2) CCL13 sensor detects CCL17; 3) CCL3 sensor detects PCSK9; 4) CXCL12alpha and beta sensors detect both isoforms; 5) IL-12p70 and IL-23 sensors detect IL-12p40. (d) Leave-some-out assay: 6 pools of recombinant proteins consisting of either all the targets in the 191-plex panel (A1) or lacking a subset of targets in the 191-plex panel (A2-A5) were profiled; boxes represent portions of the heatmap where no signal is expected due to the absence of the target proteins; colors represent SNR. (e) Overlaid standard curves for 1 example CLAMP using (red) standard and (blue) extended dynamic range (xDR) protocols. (f) Distribution of SNR values for all 191-plex across 80 cell culture supernatants from stimulated PBMCs quantified using (red) standard or (blue) xDR protocols. (g) Distribution of the lower limits of detection (LLOD, green) and upper limits of detection (ULOD, red or blue) of 191 sensors using (red) standard or (blue) xDR protocols. (h) Distribution of coefficients of variation (percent CV) of all nELISA sensors in repeat measurements of a single sample across wells in a single plate (well-to-well, blue) and across plates profiled on different days (day-to-day, red). (i) Cell culture supernatants from stimulated PBMCs were analyzed on the nELISA platform and the traditional xMAP multiplex ELISA platform; shown are the distribution of spearman correlation coefficients for shared sensors with detectable protein concentrations, and an example correlation of protein concentrations across samples for IL-1b (inlaid). (j) Cross-reactivity comparison on xMAP and nELISA platforms: 100 recombinant antigens were pooled and spiked in cell culture media at increasing concentrations; shown are the quantification of 7 proteins ***not present*** in the sample using the nELISA (top) and xMAP (bottom).

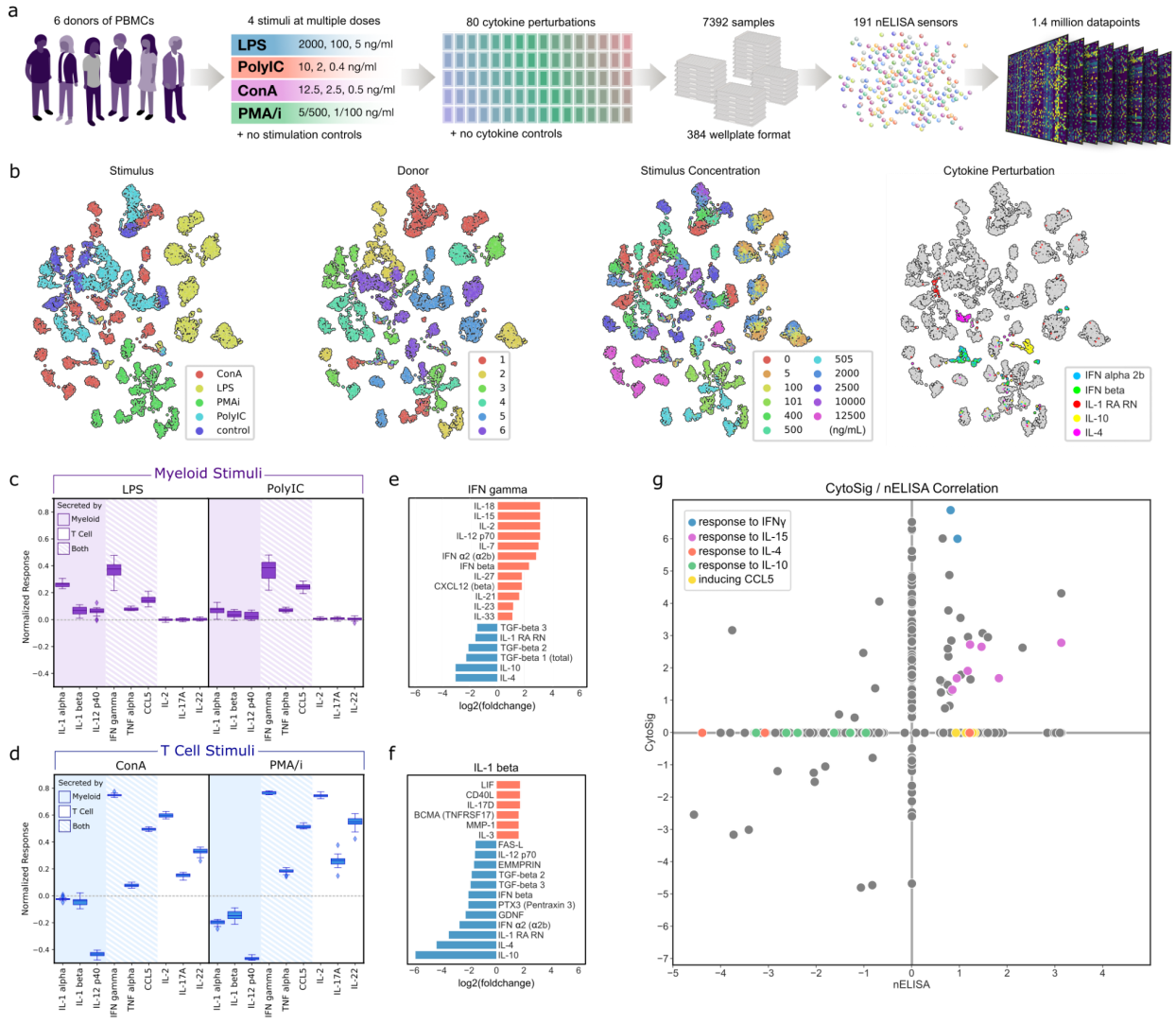

Figure 3: High-throughput screen of PBMC responses demonstrates the use of the nELISA for drug discovery. (a) Screen design: PBMCs isolated from 6 donors were treated with inflammatory stimuli at indicated concentrations, and further perturbed with 80 recombinant cytokine "perturbagens", generating a total of 7,392 samples; after 24 hours, concentrations of 191 secreted proteins were measured in the supernatant of each sample using the nELISA. (b) UMAP dimensionality reduction of the entire nELISA dataset; datapoints are colored (from left to right) by stimulation condition, by donor, by stimulation concentration, or by individual cytokine perturbagens with strong effects, as indicated. (c) PBMC expression of indicated proteins, in response to myeloid stimuli (LPS or PolyIC), in the absence of recombinant cytokine perturbagens. (d) PBMC expression of indicated proteins, in response to T cell stimuli (ConA or PMA/i), in the absence of recombinant cytokine perturbagens. (e-f) Fold change in the expression of IFNg (e) and IL-1 beta (f) in response to indicated perturbagens, across all donors and stimulation conditions. (g) Correlation between cytokine interactions detected by nELISA and CytoSig in PBMCs, according to the fold change in expression of a protein in response to a perturbagen. Examples of cytokine interactions are indicated: response to IFNg (blue), response to IL-15 (purple), response to IL-4 (red), response to IL-10 (green), perturbagens inducing CCL5 (yellow).

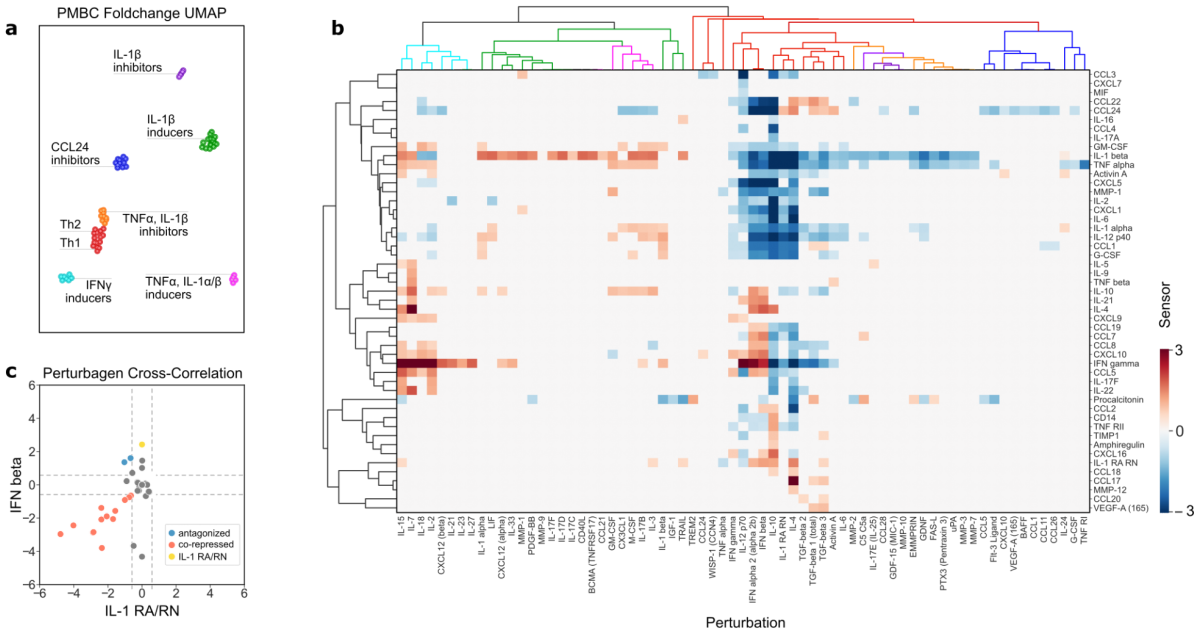

Figure 4: nELISA reveals biological insights from cell-based screens. (a) UMAP of PBMC secretome phenotypes in response to perturbagens, compiled across all stimulation and donor conditions; clusters are labelled according to shared features in PBMC secretomes. (b) Heatmap dendrogram of perturbagen effects on cytokine expression across all stimulation and donor conditions; colors indicate fold change for each sensor over no perturbagen control. (c) Correlation between significant effects of IFNb and IL-1 RARN on unstimulated PBMCs. Shown are cytokines inhibited by both perturbagens (red), cytokines induced by IFNb but inhibited by IL-1 RARN (blue), and the induction of IL-1 RARN by IFNb (green).

References

1. Cayer, D. M., Nazor, K. L. & Schork, N. J. Mission critical: the need for proteomics in the era of next-generation sequencing and precision medicine. *Hum. Mol. Genet.* **25**, R182–R189 (2016).
2. Juncker, D., Bergeron, S., Laforte, V. & Li, H. Cross-reactivity in antibody microarrays and multiplexed sandwich assays: shedding light on the dark side of multiplexing. *Curr. Opin. Chem. Biol.* **18**, 29–37 (2014).
3. Assarsson, E. *et al.* Homogenous 96-plex PEA immunoassay exhibiting high sensitivity, specificity, and excellent scalability. *PLoS One* **9**, e95192 (2014).
4. Gold, L., Walker, J. J., Wilcox, S. K. & Williams, S. Advances in human proteomics at high scale with the SOMAscan proteomics platform. *N. Biotechnol.* **29**, 543–549 (2012).
5. Pla-Roca, M. *et al.* Antibody colocalization microarray: a scalable technology for multiplex protein analysis in complex samples. *Mol. Cell. Proteomics* **11**, M111.011460 (2012).
6. Laforte, V., Lo, P.-S., Li, H. & Juncker, D. Antibody Colocalization Microarray for Cross-Reactivity-Free Multiplexed Protein Analysis. *Methods Mol. Biol.* **1619**, 239–261 (2017).
7. Paquet-Mercier, F., Juncker, D. & Bergeron, S. Precise Chip-to-Chip Reagent Transfer for Cross-Reactivity-Free Multiplex Sandwich Immunoassays. *Methods Mol. Biol.* **2237**, 141–149 (2021).
8. Dagher, M., Kleinman, M., Ng, A. & Juncker, D. Ensemble multicolour FRET model enables barcoding at extreme FRET levels. *Nat. Nanotechnol.* **13**, 925–932 (2018).
9. Tighe, P. J., Ryder, R. R., Todd, I. & Fairclough, L. C. ELISA in the multiplex era: potentials and pitfalls. *Proteomics Clin. Appl.* **9**, 406–422 (2015).
10. Wilson, R., Cossins, A. R. & Spiller, D. G. Encoded microcarriers for high-throughput multiplexed detection. *Angew. Chem. Int. Ed Engl.* **45**, 6104–6117 (2006).
11. Strengell, M. *et al.* IL-21 in synergy with IL-15 or IL-18 enhances IFN-gamma production in human NK and T cells. *J. Immunol.* **170**, 5464–5469 (2003).
12. Borger, P., Kauffman, H. F., Postma, D. S. & Vellenga, E. IL-7 differentially modulates the expression of IFN-gamma and IL-4 in activated human T lymphocytes by transcriptional and post-transcriptional mechanisms. *J. Immunol.* **156**, 1333–1338 (1996).
13. Le, J., Lin, J. X., Henriksen-DeStefano, D. & Vilcek, J. Bacterial lipopolysaccharide-induced interferon-gamma production: roles of interleukin 1 and interleukin 2. *J. Immunol.* **136**, 4525–4530 (1986).
14. Kohno, K. *et al.* IFN-gamma-inducing factor (IGIF) is a costimulatory factor on the activation of Th1 but not Th2 cells and exerts its effect independently of IL-12. *J. Immunol.* **158**, 1541–1550 (1997).
15. Peleman, R., Wu, J., Fargeas, C. & Delespesse, G. Recombinant interleukin 4 suppresses the production of

interferon gamma by human mononuclear cells. *J. Exp. Med.* **170**, 1751–1756 (1989).

16. D'Andrea, A. *et al.* Interleukin 10 (IL-10) inhibits human lymphocyte interferon gamma-production by suppressing natural killer cell stimulatory factor/IL-12 synthesis in accessory cells. *J. Exp. Med.* **178**, 1041–1048 (1993).
17. Jiang, P. *et al.* Systematic investigation of cytokine signaling activity at the tissue and single-cell levels. *Nat. Methods* **18**, 1181–1191 (2021).
18. Czimmerer, Z. *et al.* The epigenetic state of IL-4-polarized macrophages enables inflammatory cistromic expansion and extended synergistic response to TLR ligands. *Immunity* **55**, 2006–2026.e6 (2022).
19. Watanabe, K., Jose, P. J. & Rankin, S. M. Eotaxin-2 generation is differentially regulated by lipopolysaccharide and IL-4 in monocytes and macrophages. *J. Immunol.* **168**, 1911–1918 (2002).
20. te Velde, A. A., Huijbens, R. J., Heije, K., de Vries, J. E. & Figdor, C. G. Interleukin-4 (IL-4) inhibits secretion of IL-1 beta, tumor necrosis factor alpha, and IL-6 by human monocytes. *Blood* **76**, 1392–1397 (1990).
21. Saraiva, M., Vieira, P. & O'Garra, A. Biology and therapeutic potential of interleukin-10. *J. Exp. Med.* **217**, (2020).
22. Swanson, B. J., Murakami, M., Mitchell, T. C., Kappler, J. & Marrack, P. RANTES production by memory phenotype T cells is controlled by a posttranscriptional, TCR-dependent process. *Immunity* **17**, 605–615 (2002).
23. Homma, T. *et al.* Cooperative activation of CCL5 expression by TLR3 and tumor necrosis factor-alpha or interferon-gamma through nuclear factor-kappaB or STAT-1 in airway epithelial cells. *Int. Arch. Allergy Immunol.* **152 Suppl 1**, 9–17 (2010).
24. Dinarello, C. A. Overview of the IL-1 family in innate inflammation and acquired immunity. *Immunol. Rev.* **281**, 8–27 (2018).
25. Panganiban, R. P., Vonakis, B. M., Ishmael, F. T. & Stellato, C. Coordinated post-transcriptional regulation of the chemokine system: messages from CCL2. *J. Interferon Cytokine Res.* **34**, 255–266 (2014).
26. Korbecki, J., Barczak, K., Gutowska, I., Chlubek, D. & Baranowska-Bosiacka, I. CXCL1: Gene, Promoter, Regulation of Expression, mRNA Stability, Regulation of Activity in the Intercellular Space. *Int. J. Mol. Sci.* **23**, (2022).
27. Fan, J., Heller, N. M., Gorospe, M., Atasoy, U. & Stellato, C. The role of post-transcriptional regulation in chemokine gene expression in inflammation and allergy. *Eur. Respir. J.* **26**, 933–947 (2005).
28. Freen-van Heeren, J. J. Post-transcriptional control of T-cell cytokine production: Implications for cancer therapy. *Immunology* **164**, 57–72 (2021).
29. Corsello, S. M. *et al.* The Drug Repurposing Hub: a next-generation drug library and information resource. *Nat. Med.* **23**, 405–408 (2017).
30. Hoffmann, A. & Bernhagen, J. Revisiting the secretion mechanism(s) of macrophage migration inhibitory

factor-welcome to the 'UPS club'. *Immunology and cell biology* vol. 98 704–708 (2020).

31. Liu, J. S. H., Amaral, T. D., Brosnan, C. F. & Lee, S. C. IFNs Are Critical Regulators of IL-1 Receptor Antagonist and IL-1 Expression in Human Microglia. *The Journal of Immunology* vol. 161 1989–1996 Preprint at https://doi.org/10.4049/jimmunol.161.4.1989 (1998).
32. Comabella, M. *et al.* Induction of serum soluble tumor necrosis factor receptor II (sTNF-RII) and interleukin-1 receptor antagonist (IL-1ra) by interferon beta-1b in patients with progressive multiple sclerosis. *Journal of Neurology* vol. 255 1136–1141 Preprint at https://doi.org/10.1007/s00415-008-0855-1 (2008).
33. Sciacca, F. L., Canal, N. & Grimaldi, L. M. Induction of IL-1 receptor antagonist by interferon beta: implication for the treatment of multiple sclerosis. *J. Neurovirol.* **6 Suppl 2**, S33–7 (2000).
34. Ozdogan, H. *et al.* The efficacy of anti- IL-1 treatment in three patients with coexisting familial Mediterranean fever and multiple sclerosis. *Mult. Scler. Relat. Disord.* **45**, 102332 (2020).
35. Lopalco, G., Schiraldi, S., Venerito, V., Guerriero, S. & Iannone, F. Effectiveness and safety profile of anakinra in a HLA-B27 positive patient with multiple sclerosis-associated uveitis. *Mult. Scler. Relat. Disord.* **42**, 102152 (2020).
36. Li, Y. *et al.* A Functional Genomics Approach to Understand Variation in Cytokine Production in Humans. *Cell* **167**, 1099–1110.e14 (2016).
37. You, K. *et al.* QRICH1 dictates the outcome of ER stress through transcriptional control of proteostasis. *Science* **371**, (2021).
38. Wang, Q. *et al.* MIF as a biomarker and therapeutic target for overcoming resistance to proteasome inhibitors in human myeloma. *Blood* **136**, 2557–2573 (2020).
39. Rivas-Fuentes, S., Salgado-Aguayo, A., Arratia-Quijada, J. & Gorocica-Rosete, P. Regulation and biological functions of the CX3CL1-CX3CR1 axis and its relevance in solid cancer: A mini-review. *J. Cancer* **12**, 571–583 (2021).
40. Laufer, J. M. & Legler, D. F. Beyond migration-Chemokines in lymphocyte priming, differentiation, and modulating effector functions. *J. Leukoc. Biol.* **104**, 301–312 (2018).
41. Righetti, A. *et al.* CXCL12 and Its Isoforms: Different Roles in Pancreatic Cancer? *J. Oncol.* **2019**, 9681698 (2019).
42. De La Luz Sierra, M. *et al.* Differential processing of stromal-derived factor-1alpha and stromal-derived factor-1beta explains functional diversity. *Blood* **103**, 2452–2459 (2004).
43. Chang, C.-W., Seibel, A. J., Avendano, A., Cortes-Medina, M. G. & Song, J. W. Distinguishing Specific CXCL12 Isoforms on Their Angiogenesis and Vascular Permeability Promoting Properties. *Adv. Healthc. Mater.* **9**,

e1901399 (2020).

44. Pawig, L., Klasen, C., Weber, C., Bernhagen, J. & Noels, H. Diversity and Inter-Connections in the CXCR4 Chemokine Receptor/Ligand Family: Molecular Perspectives. *Front. Immunol.* **6**, 429 (2015).
45. Molon, B. *et al.* T cell costimulation by chemokine receptors. *Nat. Immunol.* **6**, 465–471 (2005).
46. Sai, J., Rogers, M., Hockemeyer, K., Wikswo, J. P. & Richmond, A. Chapter Two - Study of Chemotaxis and Cell–Cell Interactions in Cancer with Microfluidic Devices. in *Methods in Enzymology* (ed. Handel, T. M.) vol. 570 19–45 (Academic Press, 2016).
47. Das, A. & Yan, L. I. 6 - ANTI-CCL-2/MCP-1: DIRECTED BIOLOGICALS FOR INFLAMMATORY AND MALIGNANT DISEASES. in *Target Validation in Drug Discovery* (eds. Metcalf, B. W. & Dillon, S.) 103–119 (Academic Press, 2007).
48. Bray, M.-A. *et al.* Cell Painting, a high-content image-based assay for morphological profiling using multiplexed fluorescent dyes. *Nat. Protoc.* **11**, 1757–1774 (2016).